Available online at www.sciencedirect.com
SCIENCE DIRECT®
ELSEVIER
Journal of Nuclear Materials 320 (2003) 245–257
journal of nuclear materials
www.elsevier.com/locate/jnucmat

Evidence for neutron irradiation-induced metallic precipitates in model alloys and pressure-vessel weld steel

Stephen E. Cumblidge [a], Arthur T. Motta [a,*], Gary L. Catchen [a], Gerhard Brauer [b], Jürgen Böhmert [c]

[a] *Department of Mechanical and Nuclear Engineering, The Pennsylvania State University, 227 Reber Building, University Park, PA 16802-1400, USA*
[b] *Institut für Ionenstrahlphysik und Materialforschung, Forschungzentrum Rossendorf, PF 510119, D-01314 Dresden, Germany*
[c] *Institut für Sicherheitsforschung, Forschungzentrum Rossendorf, PF 510119, D-01314 Dresden, Germany*

Received 6 August 2002; accepted 3 March 2003

Abstract

We have used positron Doppler-broadening spectroscopy to examine a series of neutron-irradiated model alloys (1×10^{23} n/m^2, $E > 0.5$ MeV) and 73W-weld steel (to 1.8×10^{23} n/m^2, $E > 1$ MeV. The copper, nickel and phosphorus content of the model alloys was systematically varied. The samples were examined in the as-irradiated state and after post-irradiation isochronal anneals to temperature up to 600 °C. By following the S and W parameters, and especially by plotting the results in (S, W) space, we can infer that the damage is a combination of irradiation-induced metallic precipitates and vacancy-type defect clusters. Samples with either high Cu or with a combination of high Ni and medium Cu (and the pressure-vessel weld steel) showed evidence for both irradiation-induced metallic precipitation, and vacancy-type clusters, while samples without either high Ni or high Cu showed predominantly evidence of annihilations in vacancy-type clusters. These results are discussed in terms of embrittlement models.

PACS: 61.80.Az; 61.80.Hg; 61.82.Bg; 61.72.Qq

1. Introduction

Current models used to explain the embrittlement of pressure-vessel steel during neutron irradiation are based on the development of a fine structure of radiation-induced defects, which hinder dislocation motion during deformation and cause embrittlement [1]. Although the exact nature of these defects is still in question, as they are not resolvable by transmission electron microscopy, it is thought that the main candidates are (i) fine irradiation-induced precipitates and (ii) defect clusters of various types and sizes, called matrix damage. These defects are very small in size and are difficult to resolve and examine using standard techniques, but they have been characterized using small angle neutron scattering (SANS) [2,3], atom probe field ion microscopy [4–6], and positron spectroscopies [7–15]. In particular, positron lifetime spectroscopies have been shown to be sensitive to both matrix damage and metallic precipitates in metals [9,16]. While positron lifetime measurements can be used to obtain information about the type and concentration of defects present in a sample, Doppler-broadening (DB) spectroscopy can be used to obtain information about the elemental composition of the region in which the positrons annihilate. In this paper we use DB spectroscopy to study a series of neutron-irradiated model alloys and one neutron-irradiated pressure-vessel steel.

Positrons are trapped by a precipitate if the difference in positron affinity between the host matrix and the

* Corresponding author. Tel.: +1-814 865 0036; fax: +1-814 865 8499.
E-mail address: atm2@psu.edu (A.T. Motta).

0022-3115/03/$ - see front matter
doi:10.1016/S0022-3115(03)00190-9

precipitate is positive and if the radius of the precipitate exceeds a critical size [17], as previously discussed for the case of reactor pressure-vessel steels [16]. Preliminary results regarding our model alloys are presented in an earlier report [9]. Further support for this preferential interaction between positrons and metallic precipitates was obtained by Nagai and co-workers [18,19] who demonstrated that a quantum-dot confinement state of positrons exists in small Cu precipitates in Fe alloys. We present new information about the nature of these defects, in particular we present evidence for the presence of precipitates rich in Cu and Ni and for the existence of small defect clusters, but not voids.

2. Experimental procedure

As described previously [9], as positron source we use a dried precipitate of ^{22}Na encapsulated in Kapton foil; the spot size was about 1 mm. The positron source consisted of 75 μCi of carrier-free ^{22}Na, surrounded by two sheets of Kapton film. For positron lifetime measurements, the 1.28 MeV γ-ray emitted following the β^+-decay of ^{22}Na provides the start signal, and the stop signal is one of the two 511-keV annihilation quanta provide the annihilation signal. To perform the measurements this positron source is interposed between two pieces of the sample such that virtually all of the positrons annihilate within the sample.

To measure positron lifetime distributions in samples with low ^{60}Co activity, we used a standard BaF_2 two-detector, fast–slow-coincidence positron-lifetime spectrometer. To examine samples with significant ^{60}Co activity, we used a modified three-detector system [20]. In the three-detector arrangement, we use a 'start' detector to detect the 1.28 MeV γ-ray emitted following the β^+-decay of ^{22}Na, one 'stop' detector to detect one of the two 511-keV annihilation quanta, and a third NaI 'check' detector, which must detect the second 511-keV annihilation quantum, coincident with the response of the stop detector, for the lifetime to be recorded. This arrangement reduces the interference caused by the two γ-rays emitted in the decays of ^{60}Co by roughly two orders of magnitude, although it reduces the counting rate. Both positron systems have a time resolution of 270 ps. The equipment was kept in a room where the temperature was well controlled to avoid electronic drift. The positron lifetime system was frequently calibrated using well-annealed Fe foils to determine the time resolution and the fraction of positrons annihilating in the source.

We used the PATFIT package to perform the deconvolution of the positron lifetime distributions [21]. We used the program RESOLUTION to analyze the lifetime distributions corresponding to a Fe foil to determine the resolution function of the system and to determine the fraction of positrons annihilating in the positron source. Using the resolution function generated for a known sample by RESOLUTION, we then used the program POSITRONFIT to perform the deconvolution of the positron lifetime distributions measured on the experimental samples.

A DB energy distribution measured on a pristine crystal consists of a 511 keV full-energy peak with two components: (i) annihilations with the tightly-bound core electrons, which have a relatively high momentum and which contribute to the broad base in the peak and (ii) events arising from annihilations with low-momentum valence electrons, which contribute to the sharper, inner component of the peak. The DB W, or 'wing', parameter provides a measure of the broad component of the annihilation-quanta lineshape by measuring the number of counts falling outside of an energy interval, set to exclude most of the sharp, inner component. Because the W-parameter represents the relative number of positrons annihilating with core electrons as opposed to valence electrons and because this quantity varies from metal to metal, the W-parameter can give compositional information about the material in the region where the positron annihilates.

For the DB measurements, we used a Ge X-ray detector with an energy resolution of 1.07 ± 0.05 keV at 511 keV. The DB spectrometer was frequently calibrated using an ^{181}Hf 482-keV γ-ray source and a ^{85}Sr 514-keV γ-ray source. We analyzed peaks corresponding to the 511 keV annihilation quanta using the Doppler lineshape S-parameter and W-parameter. We defined the S-parameter as the ratio of the counts that fall within 1 keV of the center of the 511-keV peak to the total number of counts under the peak. We defined the W-parameter as the ratio of the number of counts that were more than 3 keV from the center of the 511-keV peak to the total number of counts under the peak. We measured the S and W-parameters in well-annealed, high-purity Fe, Cu, and Ni samples to obtain reliable standards for these metals [9]. The purities of the elements used for this benchmarking were 99.5% Fe, 99.98% Ni, and 99.99+% Cu.

Generally, for the DB energy distributions, we collected enough events so that the effects of counting statistics were insignificant. Thus the primary uncertainties in the S and W values arose from systematic effects, which a priori are not simple to estimate. To determine the extent of systematic error for a set of S- or W-values we observed fluctuations from measurement to measurement which were made under physical conditions for which no variation in S- or W would be expected. An example is a set of measurements after low temperature anneals (<300 °C). We found using this approach that the variations in S and W are relatively small (see Figs. 4–7), which would suggest a small systematic error in our experiments.

Table 1
Model alloy chemical composition (wt%)

Material	C	S	Cu	P	Ni	Si	Mn	Cu/P/Ni
A	0.01	0.004	0.02	0.002	0.01	0.15	0.39	LLL
B	0.01	0.005	0.42	0.012	0.01	0.24	0.49	HML
C	0.01	0.004	0.12	0.010	1.98	0.09	0.35	MMH
D	0.01	0.004	0.12	0.012	1.10	0.12	0.41	MMM
E	0.01	0.004	0.12	0.039	1.13	0.2	0.46	MHM
F	0.01	0.004	0.42	0.012	1.19	0.21	0.47	HMM

Table 1 gives the compositions of the eight model alloys used in this study [22]. The amounts of nickel, copper, and phosphorus were systematically varied in these alloys. The amounts of copper, phosphorus, and nickel are abbreviated in the last column as high (H), medium (M) or low (L). Material A represents a baseline, with low concentrations of copper, nickel, and phosphorus. Material D represents a midline sample, with medium concentrations of copper, nickel, and phosphorus. Samples C, E and F are variations of D, with high amounts of one element. B is similar to A but with high Cu and medium P concentrations. The alloys were austenitized at 980–1000 °C for 2 h and then oil quenched. They were then tempered at 670 °C for 10 h, and then were cooled in air. The samples were originally in the form of Charpy V-notch test specimens, and were cut into 1 $cm^2 \times 1$ mm slices with a wafering diamond blade. The samples were etched with nitric acid to remove the near surface cold-worked region, created by the cutting, polishing, and grinding operations.

Alloys A–F were irradiated to 1×10^{23} n/m^2 ($E > 0.5$ MeV) at the ROVNO-1 commercial reactor at a flux of 4×10^{15} n/m^2 s. Samples of materials A and B were also irradiated at the KOLA-3 commercial reactor to 8×10^{23} n/m^2 ($E > 0.5$ MeV) at a flux of 3×10^{16} n/m^{2}s. All samples were irradiated at 270 °C. We also examined irradiated and non-irradiated 73W-weld steel, obtained from Oak Ridge National Laboratory (composition shown in Table 2). The 73W-weld steel received a post-weld heat treatment at 607 °C for 40 h. The samples were originally in the form of Charpy V-notch test specimens, and were cut into 1 $cm^2 \times 1$ mm slices with a wafering diamond blade. The 73W-weld steel was irradiated to a fast fluence of 1.8×10^{23} n/m^2 ($E > 1$ MeV) at 290 °C.

Table 2
Pressure-vessel steel (73W-weld) chemical composition (wt%)

C	0.098
S	0.005
Cu	0.31
P	0.005
Ni	0.60
Si	0.45
Mn	1.56

The model alloys and steel samples were isochronally annealed for 30 min in sealed quartz tubes filled with ultra-high-purity argon at successively higher temperatures up to 600 °C. The 73W steel was annealed in flowing ultra-high-purity argon. The non-irradiated samples were also given the same annealing procedure to provide a baseline comparison to the results obtained from annealing the irradiated samples. The samples were etched in hydrochloric acid after each annealing to remove any surface oxidation and to ensure a clean, uniform surface. They were examined using Rockwell hardness testing, and DB and positron lifetime spectroscopies after each annealing step. This annealing procedure was used to determine the temperature at which different irradiation-induced features anneal.

We measured the 15N Rockwell hardness of the samples using an American Chain and Cable Company model 6TT Rockwell hardness tester. Before each measurement, the tester was checked for accuracy using a standard test block of known hardness. In testing each sample, we performed five hardness measurements, and used the mean value and recorded the error as the standard deviation of the five measurements. These measurements were performed before and after irradiation and after each annealing step, to provide a measure of the change in mechanical properties of the samples in each condition.

3. Results

The Rockwell hardness in the model alloys is in broad agreement with the previous measurements of mechanical properties on these alloys, i.e., alloy A is the softest, followed by alloy B; alloys C–F have similar hardness in the non-irradiated state, and the 73W steel is the hardest of all. The hardness of all of the samples increased after irradiation. After annealing, the hardness decreases, approaching the pre-irradiation values. These results are shown in Fig. 1. It is clear from the figure that annealing without irradiation has little effect on the Rockwell hardness of the samples, with the exception of sample D, whose hardness decreases with annealing. The reason for this sensitivity to thermal annealing is not

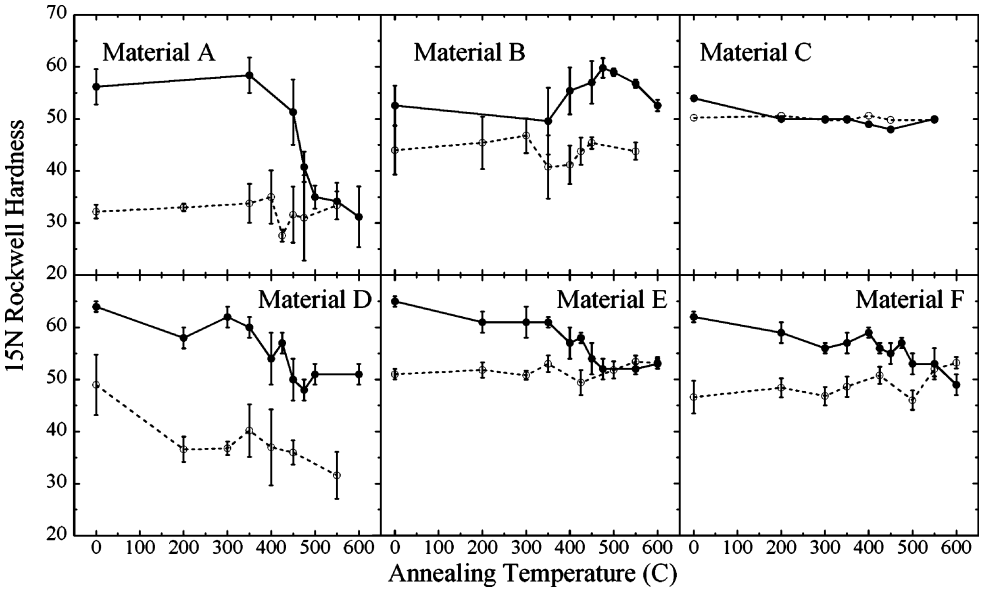

Fig. 1. 15N Rockwell hardness measured as a function of cumulative anneals at the temperatures indicated starting from the as-fabricated state (○) and from the as-irradiated state (●, fluences as described in the text) for the model alloys A–F.

known. It is noteworthy that Fig. 2 shows a significant decrease in the average positron lifetime of alloy D after annealing at 200 °C, which also corresponds to the largest decrease in hardness. Likewise after the initial increase in hardness after irradiation, post-irradiation annealing causes the hardness to decrease. For alloy A, this decrease occurs above 400 °C, while for the other alloys this decrease is more gradual. For example, for annealing temperatures between 300 and 600 °C the hardness values of alloys E and F decrease gradually to the non-irradiated values. The one exception to this trend is alloy B, in which the hardness increases between 400 and 500 °C, before decreasing again. We discuss this in more detail below.

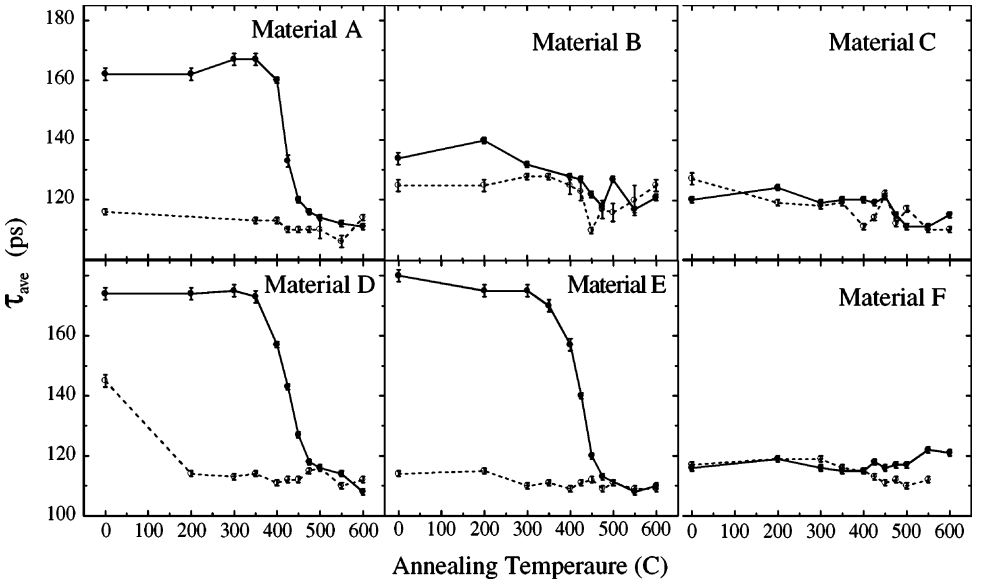

Fig. 2. Average positron lifetime measured as a function of cumulative anneals at the temperatures indicated starting from the as-fabricated state (○) and from the as-irradiated state (●, fluences as described in the text) for the model alloys A–F.

Fig. 2 shows the positron-lifetime results for the samples that were (i) annealed (open circles) and (ii) irradiated and annealed (filled circles) [9]. With the exception of sample A (see below), we report here the average positron lifetimes because given the presence of multiple lifetimes after irradiation, we could not unambiguously deconvolute the individual lifetimes. The average lifetimes give a fit-independent measure of the positron lifetimes in the material. As a result, when multiple lifetimes are present, the reported average lifetime is a combination of the individual lifetimes, weighted by their number density and sink strength for positrons.

Three of the alloys (A, D and E) show significant increases in the average positron lifetime measured after irradiation, while others (alloys B, C and F) exhibit little increase. No evidence of large voids or vacancy clusters was found in the deconvolution of the positron lifetime distribution obtained from sample A: in several deconvolution tries after irradiation the maximum positron lifetime obtained was 200–210 ps [23]. Post-irradiation annealing causes the average positron lifetimes of alloys A, D and E to decrease after annealing in the 400–450 °C temperature range, and has comparatively little effect on alloys B, C and E. Thermal annealing causes little change to the lifetimes for the alloys up to annealing temperature of 600 °C, except for alloy D, as noted above. After annealing to 550–600 °C, the average positron lifetime of the irradiated and annealed alloys is indistinguishable from that of the annealed alloys. The average positron lifetime for the 73W steel samples shows only a small increase after irradiation. Thermal annealing causes little change to the lifetimes on the non-irradiated 73W steel samples. Post irradiation annealing between 300–450 °C causes a pronounced decrease in the average positron lifetime, followed by a corresponding increase between 450 and 600 °C which brings the average positron lifetime to a value close to the value measured in the thermally-annealed sample. Similar results have been previously reported for neutron irradiated LWR A533b pressure-vessel steel [10] and for VVER pressure-vessel steel [8].

The interpretation of these results is as follows: neutron irradiation causes both defect clusters and irradiation-induced precipitates to form in the model alloys. Essentially all alloys should exhibit irradiation-induced open-volume defects (vacancy clusters, dislocation loops, depleted zones) that tend to increase the average positron lifetime. In the alloys with higher amounts of Cu and Ni, the effects of irradiation-induced precipitation can become significant; annihilations in Cu- or Ni-rich precipitates occur with a lifetime around 110–120 ps. The average positron lifetime is then determined by the relative sink strengths of the different positron traps: in samples with little amounts of Cu or Ni, the vacancy clusters dominate and the average lifetime increases with irradiation, while little increase in average lifetime is seen in samples with significant precipitation. According to this interpretation, alloys B, C and F exhibit significant irradiation-induced precipitation, while, in alloys A, D and E, most of the annihilations take place in defect clusters.

Fig. 3 shows the analogous Rockwell hardness and positron lifetime results for the 73W weld steel. The interpretation of the positron lifetimes in the 73W steel is more complex. The basic behavior is similar to that for alloys in which irradiation-induced precipitation has taken place, i.e., only a small increase in lifetime with irradiation. The positron lifetime measured after irradiation results from positron signals from annihilations in both defect clusters and in small irradiation-induced precipitates. As the irradiated alloy is annealed, the defects that constitute the irradiation-induced matrix damage start to become mobile and to annihilate at fixed sinks, causing more positrons to annihilate in the precipitates. This causes the average lifetimes to approach that of pure Cu. The explanation for the increase in the average lifetime measured after annealing at 450–600 °C is not straightforward, but one possibility is that the small irradiation-induced precipitates grow, causing them to be less efficient positron traps. This growth process could also cause the precipitates to lose coherency, creating defects at the interface that would trap the positrons, again increasing the positron lifetime. It is also possible that the precipitates simply dissolve at that

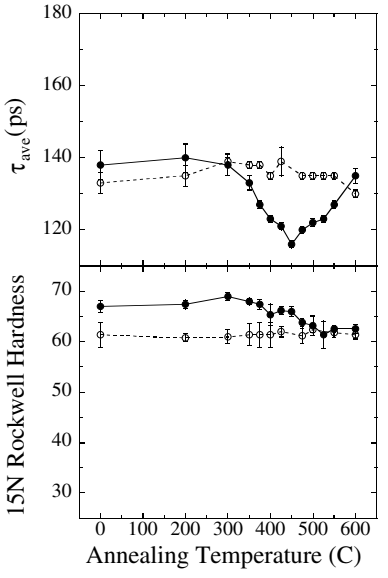

Fig. 3. Average positron lifetime and 15N Rockwell hardness measured as a function of cumulative annealing temperature starting from the as-fabricated state (○) and from the as-irradiated state (●, fluences as described in the text) for the irradiated steel 73W.

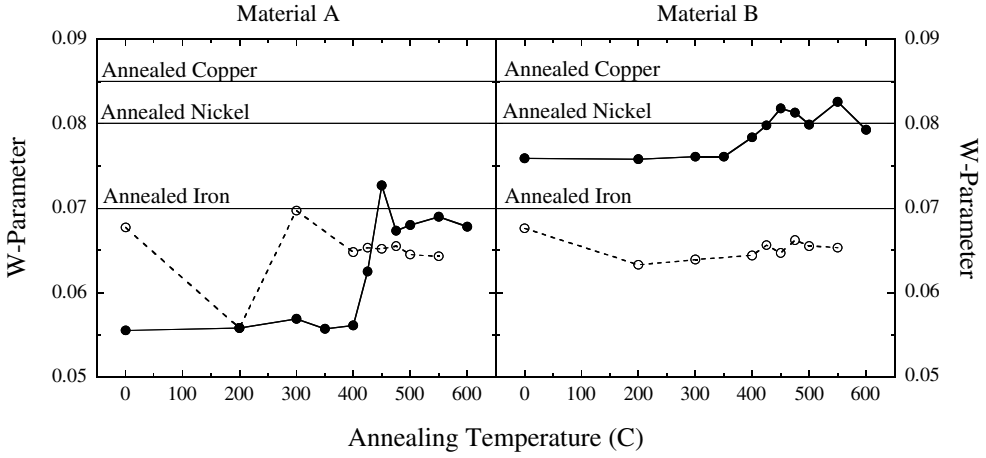

Fig. 4. DB W-parameter measured as a function of cumulative half hour anneals at the temperatures indicated starting from the as-fabricated state (○) and from the as-irradiated state (●, 1×10^{23} n/m^2, $E > 0.5$ MeV) for the model alloys A and B.

temperature – but this dissolution would not explain the increase in mean positron lifetime.

For samples A and B, Fig. 4 shows the results of the measurements of the W-parameter, measured before and after irradiation and after each successive isochronal annealing step. For sample A, which has a low concentration of the alloying elements, the W-parameter of the non-irradiated material is close to that measured in pure annealed Fe. After irradiation the W-parameter for sample A decreases significantly, and remains relatively constant upon post-irradiation annealing to temperatures up to 400 °C. Between 400 and 500 °C, the W-parameter returns to values close to those observed on the non-irradiated materials.

This behavior has a straightforward interpretation: during irradiation, vacancy-type defect clusters are formed throughout the material causing embrittlement. Because alloy A is essentially pure Fe, we ascribe this average lifetime to a combination of vacancy type defect clusters that form as a result of displacement damage. Hempel et al. [14] measured the positron lifetime as a function of defect cluster size in iron. Their results indicate that the defect clusters with a lifetime of 200–210 ps (responsible for trapping the positrons in the irradiated sample A) contain on the average 2–3 vacancies. Other researchers have observed somewhat larger clusters (5–6 defects) in VVER-type steels [24]. If only one lifetime was present, this lifetime would indicate the size of the vacancy clusters (assuming that the chemistry in our pure Fe alloys is similar to that in the Hempel study), however it is more likely that the measured average lifetime represents a mixture of lifetimes characteristic of a combination of defect clusters. These vacancy-type defect clusters are likely to consist of a combination of small vacancy clusters, small dislocation loops, or depleted zones: the observed average lifetime depends on the exact combination of defects left as a result of cascade debris. As mentioned above, there is little evidence of large voids or defect clusters. We designate the ensemble of these irradiation-induced defects as 'matrix damage', as this is a term commonly used to describe these defects.

The momentum distribution of the annihilation quanta produced by the positrons that annihilate at these 'matrix damage' defects is narrower than that produced by the positrons that annihilate in the bulk material. Because the concentration of these defects increases during irradiation, the W-parameter *decreases* for measurements performed after irradiation. Following irradiation a larger percentage of the annihilations takes place in defects. After annealing around 450 °C, the defect clusters disappear as the defects become mobile and are absorbed into the sinks in the material. This decrease causes the percentage of annihilations in these defects to decrease, and the W-parameter increases back to a value close to that for annealed Fe. This interpretation is supported by the increase in the hardness in material A measured after irradiation, as these irradiation-induced defects cause irradiation hardening. As mentioned above, the irradiation-induced increase in hardness also disappears at about 450 °C, indicating that the material is close to its pre-irradiated condition.

For the non-irradiated sample B (which has a high Cu concentration), the W-parameter is also close to the bulk iron value; but, in contrast to sample A, it increases significantly after irradiation. As shown in Fig. 4, in the as-irradiated sample, the value of the W-parameter is in-between the values observed in the as-irradiated sample A and the value for annihilations observed in pure Cu, but closer to the latter. Annealing causes the W-parameter to increase further, then to start decreasing around 600 °C. As the annealing temperature increases

to 450 °C, the W-parameter approaches the value for annihilations in pure Cu.

These observations can be interpreted by assuming the development in sample B of a fine distribution of Cu-rich precipitates, in parallel with the aforementioned vacancy-type defect clusters. The positrons are trapped within the Cu precipitates, because the positron affinity in Cu is greater than in Fe. In fact, the difference in positron affinity is high enough both for the irradiation-induced precipitates and the defect clusters that they act as 'black holes' to the positrons (i.e. de-trapping is unlikely [16,25]). As a result, the observed W-parameter in the as-irradiated sample B likely results from a mixture of positron annihilations at defect clusters and precipitates. As the annealing temperature increases to 450–500 °C, the defect clusters disappear as in sample A. Whereas, in sample A, the disappearance of the defect clusters causes the percentage of annihilations in the bulk to increase; and in sample B, the disappearance of the defect clusters causes an increase in the trapping of the positrons by metallic precipitates. This decrease in annihilations in defect clusters causes the percentage of annihilations occurring in Cu-rich precipitates to increase and the W-parameter to approach the value for annihilations in pure Cu. The fact that the W-parameter value does not exactly match the W-parameter value for pure Cu is consistent with the observations of others who have ascribed a mixed chemistry to these precipitates [2,4]. As mentioned above, the hardness of sample B increases after annealing at 400 °C. This increase could be caused by additional precipitation from solid solution, causing the precipitates to increase in number, in size, or both. It is not clear what the role of precipitate evolution could have on this picture; if the precipitates became incoherent in the temperature range of 550 °C, this would be consistent with the small positron lifetime increase seen (Fig. 2). The slight decrease in the W-parameter, when the temperature approaches 600 °C could be caused by the onset of precipitate dissolution or to Ostwald ripening, which would decrease the overall sink strength of the Cu-rich precipitates. We note that the sample hardness does not return to the pre-irradiated values, after annealing at 600 °C, which means that annealing does not completely eliminate the irradiation-induced microstructures.

Fig. 5 shows the corresponding results obtained for samples C and D. Sample C is a high Ni, medium Cu alloy. For that sample, the W-parameter increases slightly after irradiation, to a value close to that characteristic of annihilations in annealed Fe. Post-irradiation annealing of sample C in the temperature range 400–500 °C causes the W-parameter to decrease. The increase of the W-parameter after irradiation could be caused by a mechanism similar to that proposed for sample B, i.e., positrons annihilate at a combination of defect clusters and irradiation-induced precipitates. The difference here is that the composition of the irradiation-induced precipitates is likely to be much richer in Ni than in sample B; and because the characteristic W-parameter for annihilations in pure Ni is lower than that for annihilations in pure Cu, we observe a lower overall value of the W-parameter for the sample. It is also possible that Ni is not as effective as Cu in catalyzing the precipitation of alloying elements from solid solution. The origin of the observed decrease of the W-parameter at 400–500 °C is not clear. One would expect an increase, given that, at this temperature, the vacancy-type defect clusters start to dissolve and to annihilate at sinks. One possibility is that Ni-rich precipitates are formed under irradiation, which are less stable than the Cu-rich precipitates and that disappear around 400–500 °C. The hardness of sample C increases modestly after

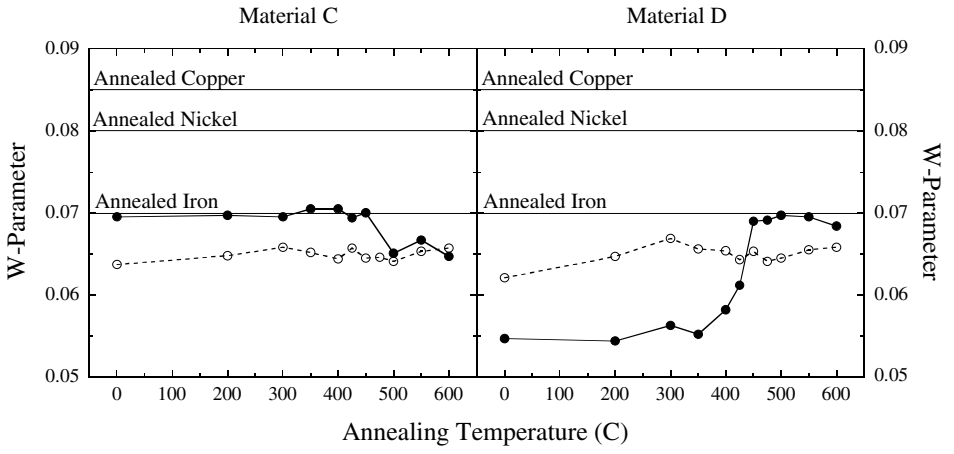

Fig. 5. DB W-parameter measured as a function of cumulative half hour anneals at the temperatures indicated starting from the as-fabricated state (○) and from the as-irradiated state (●, 1×10^{23} n/m^2, $E > 0.5$ MeV) for the model alloys C and D.

irradiation, and decreases after annealing at temperatures higher than 500 °C.

In sample D, which is similar to sample C, but with a lower Ni content, irradiation causes W to decrease (similarly to sample A) indicating the appearance of defect clusters and less irradiation-induced precipitates than appear in sample C. Fig. 5 shows that the W-parameter *decreases* after irradiation, suggesting that most annihilations are taking place in defect clusters, with little irradiation-induced metallic precipitates present to trap positrons. Thus, the irradiation of sample D, which has a lower Ni concentration, creates a lower concentration of irradiation-induced precipitates than in sample C. This difference indicates that Ni is less-efficient than Cu in creating precipitates, because measurements on a sample with a concentration of 1.1% Ni (alloy D) indicates less precipitates are formed after irradiation than do the measurements performed on a sample with only 0.42% Cu (alloy B). This interpretation is supported by the positron lifetimes shown in Fig. 2. After irradiation of sample D, the positrons annihilate mainly at defect clusters corresponding to longer lifetimes, while in after irradiation of sample C, the average positron lifetime barely changes, indicating positron trapping takes place in metallic precipitates, to which a smaller positron lifetime corresponds. Because of this lower precipitate density, the annihilations are dominated by trapping in vacancy-type defect clusters; and thus, the behavior of the W-parameter is similar to that observed on sample A. Annealing at 400–500 °C causes the W-parameter to increase to values that are slightly higher than those measured on the non-irradiated samples. This result is consistent with the vacancy-type defect clusters disappearing at ~450 °C. We interpret the results as coming from a mix of annihilations in various sinks. Comparing the high temperature W parameter measured in B with that measured in C and D, we notice the latter is lower, and we note that this is consistent with a greater Ni content in the precipitates.

Fig. 6 shows the W-parameter measurements for samples E and F. Sample E is essentially identical to sample D, except that the P content is three times higher in E than in D. The W-parameter measurements and hardness measurements for sample E are very similar to those for sample D, indicating that phosphorus does not cause significant microstructural changes at this composition, at least as measured by the W-parameter. This feature is also true of the positron lifetimes corresponding to D and E (shown in Fig. 2), which exhibit very similar behavior. Because of this similarity, the interpretation of the W-parameter and hardness results for sample E is similar to that for sample D. In sample F, which has medium Ni concentration and high Cu concentration, the W-parameter increases moderately with irradiation, similarly to samples B (high Cu) and C (high Ni, medium Cu). Further post-irradiation annealing causes the W-parameter to increase further, similarly to the other high Cu sample, (sample B). The difference is that the increase starts at a lower temperature (200 °C), and that the W-parameter value decreases (rather than increases) above 450 °C. One possible explanation is that the higher alloying element content of sample F causes a greater amount of precipitation. The greater precipitate number density then dominates the trapping, so that the positrons do not find the defect clusters. Thus they annihilate only in irradiation-induced precipitates. This situation causes the values of the W-parameter to increase after irradiation. As seen in previous studies of high Ni, high Cu steels, the high Ni catalyzes the formation of a higher density of smaller precipitates [2]. These more numerous and smaller precipitates would be more susceptible to Ostwald ripening

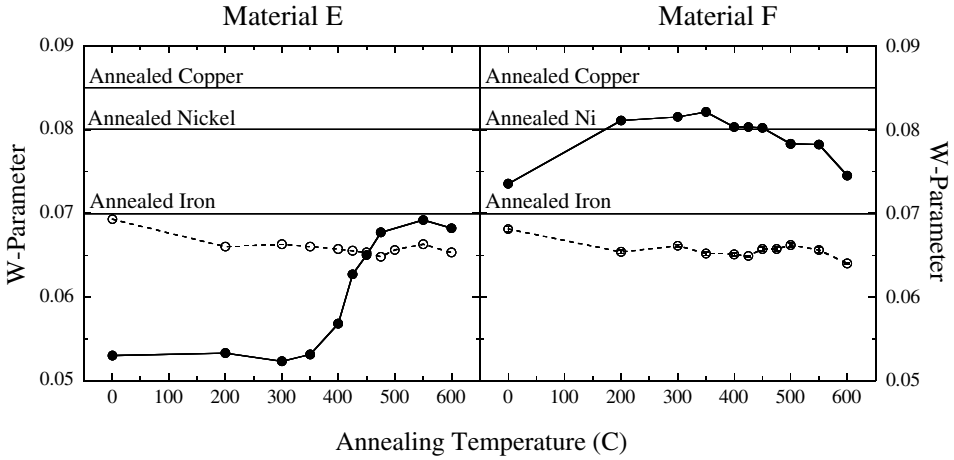

Fig. 6. DB W-parameter measured as a function of cumulative half hour anneals at the temperatures indicated starting from the as-fabricated state (○) and from the as-irradiated state (●, 1×10^{23} n/m^2, $E > 0.5$ MeV) for the model alloys E and F.

than the larger precipitates found in a low Ni material. In general, fewer, larger precipitates, even having the same total precipitated volume fraction, are less attractive to positrons than many, smaller precipitates [26] and would also cause less hardening. Once Ostwald ripening takes place, less annihilations take place in the precipitates, causing the W-parameter to approach that of annealed Fe. This hypothesis is supported by the hardness results, which show that the hardness of the material increases after irradiation, and decreases to the pre-irradiated values after annealing at 600 °C.

Fig. 7 shows the results of the measurements of the W-parameter in the 73W-weld materials. The measurements indicate that the W-parameter increases after irradiation, to a value near that measured for well-annealed Fe. Annealing causes the W-parameter of the irradiated sample to increase around 400–450 °C. This increase is consistent with the interpretation given above for the behavior of the W-parameter in sample B, i.e., a mixture of annihilations in defect clusters and in Cu-rich precipitates. As the annealing temperature increases to 400–450 °C, the defect clusters disappear, which causes a greater fraction of the positrons to be trapped by and annihilated at metallic precipitates. As this fraction increases, the W-parameter values approach a value characteristic of the local chemistry of the precipitates. After this annealing stage, the W-parameter increases to values close to those observed in measurements performed in pure Ni, likely as a result of mixed precipitate chemistry (Fe, Cu, Ni, P, etc.). The hardness of the 73W-weld sample drops after annealing to 450–500 °C, which is consistent with the overall decrease of irradiation-induced defects that occurs at this annealing temperature. Above 450 °C the W-parameter decreases, which could be caused by the dissolution of the particular type of precipitates formed in the 73W sample under irradiation. Alternatively, a certain concentration of dislocation defects present in the steel prior to irradiation, could remain in the matrix after annealing at 450 °C. If the irradiation-induced precipitates underwent Ostwald ripening, their ability to trap positrons would be impaired relative to the ability of the vacancy-type defect clusters to do the same, causing a higher percentage of precipitates to annihilate at vacancy-type defect clusters and thus causing the W-parameter to decrease. We note that both explanations would reduce the overall number of defects in the matrix and would reduce hardening. Finally, as has been suggested before [8], changes in pre-existing precipitate microstructure could account for some of these changes in the commercial alloy.

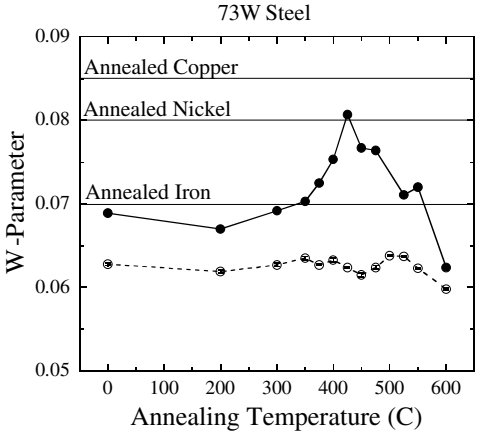

Fig. 7. DB W-parameter measured as a function of cumulative half hour anneals at the temperatures indicated starting from the as-fabricated state (○) and from the as-irradiated state (●, 1.5×10^{23} n/m^2, $E > 1$ MeV) for the 73W irradiated steel.

4. Discussion

In discussing the significance of the current results, a note of caution should be expressed, because the reproducibility of these results from sample to sample, and within various locations within the same sample needs to be verified. By the very nature of the work a small amount of material is taken to be representative of the whole. Issues such as variations in the fabrication procedures, inhomogeneities, could influence the results. Nevertheless, the measurements exhibit several remarkable features as a whole, of which we try to present a coherent picture in the following discussion.

The model alloys in this study have also been characterized by SANS and by Charpy and tensile tests [9,22]. The mechanical tests show that irradiation causes hardening and embrittlement of all of the alloys, and post-irradiation annealing at around 500 °C causes such changes largely to disappear. Bohmert and co-workers [22] also show that higher alloying content alloys exhibited high A ratios, characteristic of irradiation-induced precipitates, in agreement with the current study.

One distinctive feature of the model alloys is that alloys having high and low Cu + Ni content show different behaviors of S- and W-parameters. This difference is most clearly shown by plotting the W-parameter versus the S-parameter for the alloys studied. The S–W plots are useful because different positron traps show unique (S, W) values and such a representation elucidates more clearly the type of microstructural evolution that is taking place [27,28]. Also, by comparing the evolution of the (S, W) values for the irradiated materials with known standards (such as pure Fe, pure Cu, etc.), we can derive conclusions about the nature of the damage. Fig. 8(a) shows the starting (S, W values) in the as-fabricated state for the alloys studied in this work, as well as the values of the (S, W) parameters obtained for

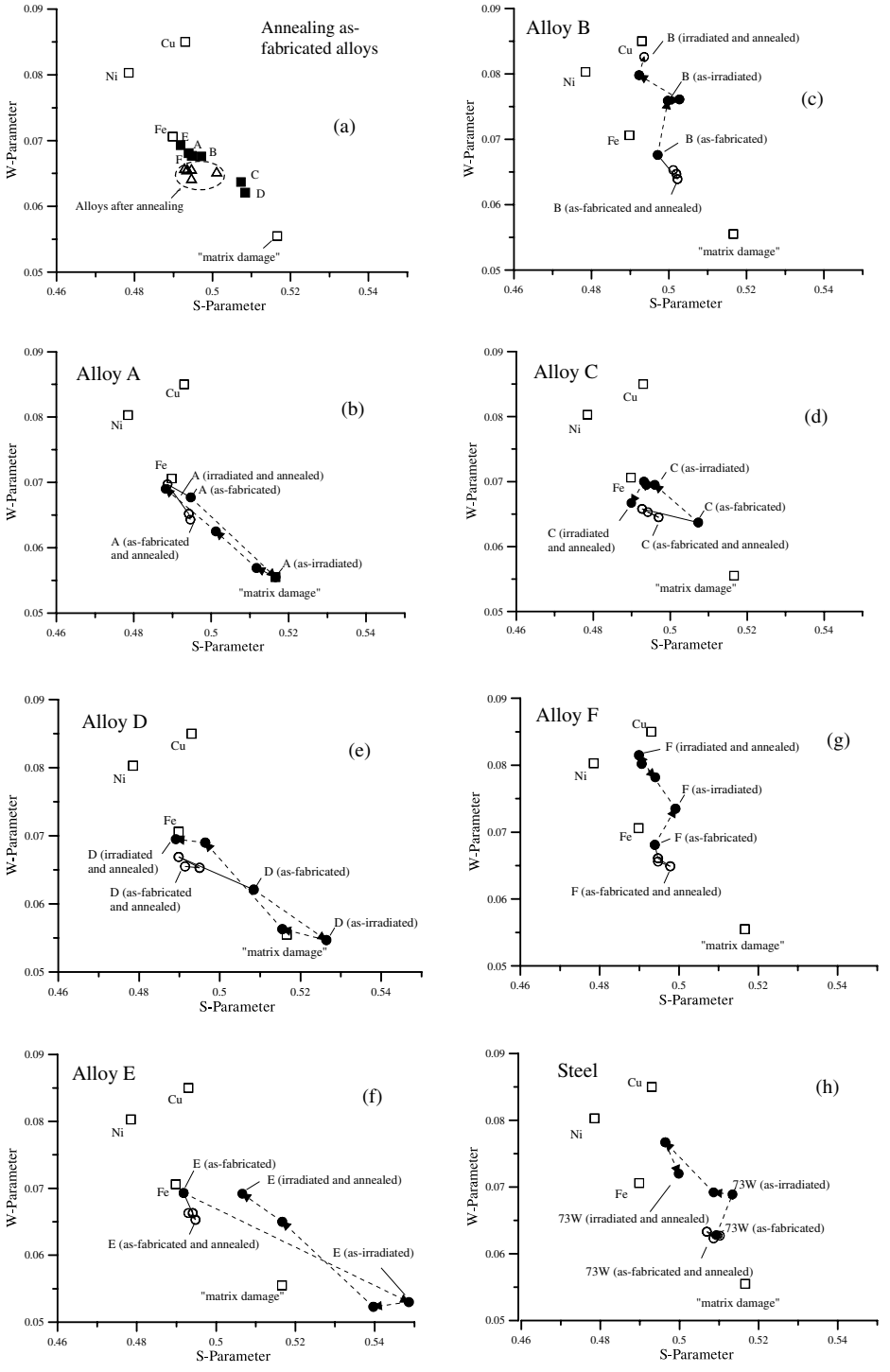

Fig. 8. Doppler-broadening S-parameter versus Doppler-broadening W-parameter for the alloys studied: (a) the (S,W) locations for all alloys in the as-fabricated state () and after annealing without irradiation. (b)–(h): Evolution of the S,W parameters for alloys A–F and 73W steel, respectively. Solid lines indicate thermal annealing to 300, 450 and 600 °C and solid circles connected by dotted arrows indicate irradiation to the fluences indicated in the text and annealing to 300, 450 and 600 °C.

non-irradiated, well-annealed Fe, Cu and Ni samples. We note that the starting (S, W) values for alloys A, B, E and F are similar, whereas those for C and D are distinct. This difference may be caused by small differences in the process history. At the end of the annealing process however, all of the alloys show up in a similar location in S, W space, suggesting a similar microstructure.

In each of the Fig. 8(b)–8(h) we show the evolution in S, W space of the samples either measured after irradiation and annealing or measured after simple thermal anneal. The arrows indicate the trajectory of the alloys, and only four points in each of the annealing process are shown for clarity:

As fabricated $\Rightarrow$ irradiation $\Rightarrow$ 300 °C anneal $\Rightarrow$ 450 °C anneal $\Rightarrow$ 600 °C anneal (black circles connected by dotted lines and arrows).

As fabricated $\Rightarrow$ 300 °C anneal $\Rightarrow$ 450 °C anneal $\Rightarrow$ 600 °C anneal (open circles connected by solid lines).

Fig. 8(b) shows this (S, W) plot for the evolution under irradiation and annealing of alloy A. In all plots we have also indicated the measured values of the pure metal standards and the 'matrix damage' point, see below. The square symbols indicate the measured pure element (Fe, Cu and Ni) benchmarks. Solid circles indicate the samples that were annealed in the as-fabricated state (i.e. without irradiation) and open circles indicate the irradiated and annealed samples. The as-fabricated material A is shown by an arrow. Starting from the arrowed point, irradiation to 1×10^{23} n/m^2 causes the S–W parameters to move to the lower right of the S–W plot (increase S and decrease W).

In an S–W plot, when only two distinct states with different annihilation characteristics (S_1, W_1) and (S_2, W_2) contribute to a set of data, we obtain a straight line, where the endpoints represent the two states [27]. For alloy A the two states are annihilations in annealed Fe and in irradiated Fe, where 'matrix damage' has been created. The successive annealing stages issue from the 'matrix damage' point and roughly follow a line that brings the S–W values back to the non-irradiated values, i.e. close to the value for annealed Fe. In effect, the S–W trajectory follows a straight line from the non-irradiated value to the value after irradiation and back close to the annealed Fe value obtained after annealing. As explained in Section 3, the annihilations in the as-irradiated material only occur in vacancy-type clusters, thus we denote that point as '*matrix damage*', and use it as a benchmark for the other samples.

The S–W plot for alloy B (Fig. 8(c)) shows quite a different story. Although the samples start from a similar location in S–W space, alloy B moves towards higher W values, and slightly higher S values. It is clear that the sample S–W values are neither moving towards the 'matrix damage' point indicated in the figure, nor are they moving towards the pure Cu point. Instead these values are going to a point in S–W space, which lies on the line between 'matrix damage' and pure Cu. If we make the simple assumption that only two traps are responsible for the annihilation of the positrons, then we would expect to find the (S, W) point after irradiation on a line traced between the 'matrix damage' and pure Cu standards as observed. (This assumes that 'matrix damage' is a combination of defect clusters and the other trap in the material are Cu-rich precipitates, here idealized as pure Cu.) Post-irradiation annealing takes the material closer to the point representative of annihilations in pure Cu likely indicating that annealing causes the 'matrix damage' to disappear from the material and therefore a large percentage of the annihilations takes place in the precipitates.

Although upon irradiation and post-irradiation annealing alloy A and alloy B show significantly different behavior, simple annealing without irradiation (open circles) causes little change in either alloy. Thus, the S–W points remain confined to a small region in S–W space and on this basis we cannot distinguish between A and B alloys. This observation indicates that without irradiation, the alloying elements do not precipitate. Cu and Ni that do not precipitate out do not affect significantly either the positron lifetime or DB characteristics because they do not trap positrons. As a result, the alloys behave similarly upon annealing without irradiation.

This pattern of (S, W) evolution is mirrored in the other alloys. Fig. 8(d)–8(g) show similar S–W plots for the other model alloys studied. The alloys that have high Cu (alloy F) or a combination of medium Cu and high Ni (alloy C), behave similarly to alloy B after irradiation, i.e., after irradiation the values of (S, W) go in the direction of increasing W and slightly increasing S. Those alloys that have neither high Cu nor a combination of medium Cu and high Ni (D and E) behave similarly to A, i.e. after irradiation, S increases substantially and W decreases. The one slight departure from this behavior is exhibited by alloy C (Fig. 8(d)), in which the S–W changes upon irradiation are smaller than those for the other alloys. Two significant differences arise between this alloy and alloys B and F: (i) the initial S–W location of the as-fabricated alloy is lower in W and higher in S than those values corresponding to the other alloys (see Fig. 8) and (ii) the alloy exhibits high Ni and medium Cu content rather than high Cu. The final state of alloy D is closer to the values for annealed Fe than the other alloys, which could indicate that the high Ni-content precipitates present in alloy D after irradiation are less stable and disappear upon annealing. Simple annealing of alloys C and D brings the (S, W) parameters close to the starting values for the other alloys. This result could indicate that in the processing of alloys C and D the microstructure was left in a less stable final state (for example, C and D could have

small amounts of cold work that is eliminated upon annealing; however metallographic examination of the as-fabricated alloys shows no visible difference). Annealing brings the microstructure of these alloys closer to that of the other alloys. Upon annealing, alloys E and F show small changes of (S, W) from the as-fabricated state.

We also note that both alloy D and alloy E show that the values of S–W evolve beyond the 'matrix damage' spot in S–W space after irradiation, even though these samples were irradiated to the same dose and under the same irradiation conditions as was alloy A. Because the results indicate that no significant precipitation has occurred, one possible explanation is that the chemistry of the defect clusters is different in these alloys. Our results do not allow us to distinguish between these possibilities.

Fig. 8(h) shows the S–W plot for the 73W steel. It is apparent from the figure that the 73W steel behaves in a similar manner to alloys B and F (high Cu alloys), indicating that the conclusions derived above for the high Cu model alloys are also valid for the steel, i.e., irradiation-induced precipitation is also an important factor in the industrial alloy. Because the chemistry of weld steel is much more complex than that of the model alloys, we would expect that the final S, W location of the irradiated steel would be different from that of the model alloys, simply because the chemistry of the precipitates would likely be also different.

It is instructive to compare the S–W plots above with the positron lifetimes presented in Fig. 2. The alloys with a S–W path similar to A (i.e. A, D and E, in which irradiation causes evolution towards lower W, high S) are the same alloys whose positron lifetimes increase after irradiation. On the other hand, the alloys with S–W similar path to B (i.e., B, C, F and 73W steel, in which irradiation causes evolution towards higher W) are the same alloys that exhibit little change in positron lifetime after irradiation. This exact correspondence of behavior gives support to the interpretation given here, which explains the results in terms of a mixture of positron annihilations in vacancy clusters and irradiation-induced precipitates.

The results shown here are in general agreement with the previously published average positron lifetime measurements [9] and with SANS results performed in the same alloys [22]. The strong interaction between irradiation-induced precipitates that likely have high Cu content is in agreement with the results of Nagai et al. [18,19], whose detailed experiments in model alloys find that positrons interact strongly with Cu clusters that are bigger than 0.6 nm. The authors find that such clusters cause the positron to be confined in a quantum-dot-like state, causing their annihilation to occur in a Cu-rich environment. Because the positron lifetime for the Cu-rich precipitates is similar to that for the bulk Fe, we cannot distinguish these precipitates from the matrix using the positron lifetime technique. In contrast, the DB measurements give much clearer information about the chemistry of the positron traps and can therefore provide independent evidence for the formation of these precipitates, which were observed by other techniques [2,5,6,29].

The present results are significant in that they provide direct independent evidence for embrittlement mechanisms previously inferred using other techniques. The fact that similar changes occurred in the weld steel as in the high alloying content model alloys suggests that the mechanisms operative in the model alloys are also operative in the steels under reactor conditions.

5. Conclusions

We have examined a series of model alloys and one pressure-vessel steel in the (i) non-irradiated, (ii) neutron-irradiated and (iii) irradiated and annealed states using DB spectroscopy and Rockwell hardness. We performed the identical annealing steps on non-irradiated samples as a control and found comparatively little effect on the positron parameters, indicating that irradiation is necessary for the observed changes. From these measurements we obtain information on the chemical composition of the defects at which positrons annihilate. In the model alloys the Cu, Ni and P contents were systematically varied. By comparing the W-parameters measured in pure metals with those measured in the materials studied, we were able to draw inferences as to the nature of the irradiation-induced defects that cause hardening and embrittlement.

The detailed results indicate:

1. A combination of irradiation-induced metallic precipitates and vacancy-type defect clusters characterizes the irradiation damage in the model alloys. The exact nature of the irradiation-induced defects depends on the sample chemistry.
2. The average positron lifetimes for the alloys A, D and E increased significantly after irradiation, while those for alloys B, C, F, and 73W steel did not. Post-irradiation annealing caused those alloys similar to A to return to non-irradiated values after annealing to 500 °C, while those for alloys similar to B exhibited little change with annealing.
3. There was a clear difference in the positron parameters of high and low alloying content samples after irradiation. In samples with high Cu concentrations, the W-parameter values showed evidence for a significant percentage of annihilations occurring at Cu- and Ni-rich metallic precipitates, whereas samples without either high Ni or high Cu concentrations showed evidence only of annihilations in vacancy-type defect clusters.

4. No effect of P was observed for samples that were otherwise identical but that had different P contents (alloys D and E).
5. Post-irradiation annealing caused the vacancy-type defect clusters to disappear upon annealing at 400–500 °C. In contrast the positron parameters associated with irradiation-induced metallic precipitates generally did not decrease until the samples were annealed at 600 °C.
6. The behavior of the pressure-vessel weld steel sample can be well understood within the same framework as that used for the model alloys, i.e. a combination of defect clusters and irradiation-induced metallic precipitates causing embrittlement.

Overall, the combination of the DB, positron lifetime and hardness results, (especially the correlation of the behavior of the alloys in *S–W* space with positron lifetime after irradiation in the low and high Cu and Ni alloys) indicate the irradiation-induced development of a combination of a fine distribution of metallic precipitates with other damage associated with vacancy-type defect clusters.

Acknowledgements

We are grateful to the FERMI group (research consortium of electrical utilities and fuel vendors, including Pennsylvania Power and Light, Philadelphia Electric Co., General Public Utilities, Commonwealth Edison, Public Services Electric and Gas and Westinghouse Electric Corporation) for sponsoring this research. We thank M. Sokolov of Oak Ridge National Laboratory for furnishing the steel samples used in this study. We acknowledge the Radiation Science and Engineering Center at Penn State, for use of the Breazeale Nuclear Reactor and other facilities and equipment.

References

[1] G.R. Odette, Scr. Metall. 17 (1983) 1183.
[2] B. Wirth, Ph.D. thesis in: Mechanical and Environmental Engineering, University of California, Santa Barbara, 1998.
[3] G. Brauer, F. Eichhorn, F. Frisius, R. Kampmann, in: Effects of Radiation on Materials: 16th International Symposium, vol. STP 1175, ASTM, 1993, p. 503.
[4] M.K. Miller, M.G. Burke, J. Nucl. Mater. 195 (1992) 68.
[5] P. Pareige, R.E. Stoller, K.F. Russel, M.K. Miller, J. Nucl. Mater. 249 (1997) 165.
[6] P. Auger, P. Pareige, S. Welzel, J.-C. van Duysen, J. Nucl. Mater. 280 (2000) 331.
[7] B.D. Wirth, P. Asoka-Kumar, R. Howell, G. Odette, P. Sterne, in: Microstructural Processes in Irradiated Materials, Materials Research Society, Boston, MA, 2001, p. R6.5.1.
[8] G. Brauer, L. Liszkay, B. Molnar, R. Krause, Nucl. Eng. Des. 127 (1991) 47.
[9] S.E. Cumblidge, G.L. Catchen, A.T. Motta, G. Brauer, J. Böhmert, in: Effects of Radiation on Materials: 20th International Symposium Williamsburg VA, vol. STP 1405, American Society for Testing and Materials, 2000, p. 247.
[10] S.E. Cumblidge, A.T. Motta, G.L. Catchen, in: Materials Research Society Symposium Proceedings, vol. 540, 1998, p. 471.
[11] S.E. Cumblidge, A.T. Motta, G. Catchen, in: Materials Research Society Symposium Proceedings, vol. 439, MRS, Boston MA, 1997, p. 483.
[12] C. Lopes-Gil, A.P. De Lima, N. Ayres de Campos, J.V. Fernandes, G. Koegel, P. Sperr, W. Trifshaeuser, D. Pachur, J. Nucl. Mater. 161 (1989) 1.
[13] K. Ghazi-Wakili, U. Zimmerman, J. Brunner, P. Tipping, W.B. Waeber, F. Heinrich, Phys. Status Solidi (a) 102 (1987) 153.
[14] A. Hempel, M. Saneyasu, Z. Tang, M. Hasegawa, G. Brauer, F. Plazaola, S. Yamaguchi, in: Effects of Radiation on Materials: 19th International Symposium Seattle, vol. STP 1366, ASTM, 1999, p. 560.
[15] R. Pareja, N. De Diego, R.M. De La Cruz, J. Del Rio, Nucl. Technol. 104 (1993) 52.
[16] G. Brauer, M.J. Puska, M. Sob, T. Korhonen, Nucl. Eng. Des. 158 (1995) 149.
[17] M.J. Puska, P. Lanki, R.M. Nieminen, J. Phys. F: Condens. Matter 1 (1989) 6081.
[18] Y. Nagai, T.Z.M. Hasegawa, T. Kanai, M. Saneyasu, Phys. Rev. B 63 (5) (2001) 134110.
[19] Y. Nagai, M. Hasegawa, Z. Tang, A. Hempel, K. Kubuta, T. Shinamura, Y. Kawazoe, A. Kawai, F. Kano, Phys. Rev. B 61 (2000) 6574.
[20] L. Van Hoorebeke, A. Fabry, E.v. Walle, J.V.d. Velde, D. Segers, L. Dorikens-Vanpraet, Nucl. Instrum. and Meth. A 371 (1996) 566.
[21] P. Kirkegaard, M. Eldrup, O.E. Mogensen, N.J. Pedersen, Comput. Phys. Commun. 23 (1981) 307.
[22] J. Böhmert, A. Ulbricht, A. Kryukov, Y. Nikolaev and D. Erak, Composition effects on the radiation embrittlement of iron alloys, Effects of Radiation on Materials: 20th International Symposium, vol. STP 1405, ASTM, Williamsburg, VA, 383.
[23] S.E. Cumblidge, Ph.D. thesis in: Nuclear Engineering, Penn State University, University Park, 2002.
[24] J. Kocik, E. Keilova, J. Cizek, I. Prochaska, J. Nucl. Mater. 303 (2002) 52.
[25] M.J. Puska, J. Phys.: Condens. Matter 3 (1991) 3455.
[26] W. Brandt, Appl. Phys. 5 (1974) 1.
[27] N. Clement, J.M.M. de Njis, P. Balk, H. Schut, A. van Veen, J. Appl. Phys. 79 (1996) 9029.
[28] H. Kauppinen, C. Corbel, L. Liszkay, T. Laine, J. Oila, K. Saarinen, P. Hautojarvi, J. Phys.: Condens. Matter 9 (1997) 10595.
[29] B.D. Wirth, G.R. Odette, W.A. Pavinich, G.E. Lucas, S.E. Spooner, in: Effects of Radiation on Materials: 18th International Symposium, vol. STP 1325, American Society for Testing and Materials, West Conshohocken, PA, 1999, p. 102.